Author/s:
Chen, J;Pan, S;Zhou, J;Lin, Z;Qu, Y;Glab, A;Han, Y;Richardson, JJ;Caruso, F

Title:
Assembly of Bioactive Nanoparticles via Metal-Phenolic Complexation

Date:
2022

Citation:
Chen, J., Pan, S., Zhou, J., Lin, Z., Qu, Y., Glab, A., Han, Y., Richardson, J. J. & Caruso, F. (2022). Assembly of Bioactive Nanoparticles via Metal-Phenolic Complexation. Advanced Materials, 34 (10), https://doi.org/10.1002/adma.202108624.

Persistent Link:
https://hdl.handle.net/11343/297434

Assembly of Bioactive Nanoparticles via Metal–Phenolic Complexation

*Jingqu Chen, Shuaijun Pan, Jiajing Zhou, Zhixing Lin, Yijiao Qu, Agata Glab, Yiyuan Han, Joseph J Richardson, and Frank Caruso**

J. Chen, Dr. S. Pan, Dr. J. Zhou, Dr. Z. Lin, Dr. Y. Qu, A. Glab, Dr. Y. Han, Dr. J. J. Richardson, Prof. F. Caruso
Department of Chemical Engineering
The University of Melbourne, Parkville, Victoria 3010, Australia
E-mail: fcaruso@unimelb.edu.au

Keywords: supramolecular assembly, functional nanoparticles, metal–organic materials, polyphenols, particle engineering

The integration of bioactive materials (e.g., proteins and genes) into nanoparticles holds promise in fields ranging from catalysis to biomedicine. However, it has been challenging to develop a simple and broadly applicable nanoparticle platform that can readily incorporate distinct biomacromolecules without affecting their intrinsic activity. Herein, a metal–phenolic assembly approach is presented whereby diverse functional nanoparticles can be readily assembled in water from combining various synthetic and natural building blocks, including poly(ethylene glycol), phenolic ligands, metal ions, and bioactive macromolecules. The assembly process is primarily mediated by metal–phenolic complexes through coordination and hydrophobic interactions, which yields uniform and spherical nanoparticles (mostly <200 nm), while preserving the function of the incorporated biomacromolecules (siRNA and 5 different proteins used). The functionality of the assembled nanoparticles is demonstrated through cancer cell apoptosis, RNA degradation, catalysis, and gene downregulation studies. Furthermore, the resulting nanoparticles can be used as building blocks for the secondary engineering of superstructures via templating and cross-linking with metal ions. The bioactivity and versatility of the platform can potentially be used for the streamlined and rational design of future bioactive materials.

1. Introduction

Recent developments in materials science have enabled the synthesis of monodisperse colloidal nanoparticles (NPs)[1] for diverse applications such as energy conversion,[2] sensing,[3] environmental remediation,[4] and biomedicine.[5] Among the various types of functional NPs, bioactive NPs (i.e., NPs containing biologically functional molecules such as proteins and genes) play a significant role in bridging nanotechnology and biotechnology by allowing the manipulation and regulation of cell behavior and biological processes.[6] Different strategies, including via physical, chemical, or biological pathways,[7–9] can be used to assemble bioactive NPs but can have associated inherent limitations. For example, assembly via physical interactions such as van der Waals and electrostatic interactions is facile but such interactions are insufficiently strong to stabilize NPs.[7] Covalent conjugation can improve the binding of biomolecules but often involves harsh synthesis conditions (e.g., organic solvents, high/low pH, toxic reagents, and/or sophisticated preparation/purification processes), which could inhibit the bioactivity of the conjugated molecules.[8] Biomolecule-directed assembly (e.g., enzyme-activated assembly) is an alternative approach that offers relatively strong and/or stable bonding specificity.[9] However, the biomolecules employed in such an approach are generally costly and can denature depending on the biological environment. Moreover, this strategy is generally biomolecule-specific because chemical specificity and degradability vary among biomacromolecules.[10] Therefore, there remains a need to develop simple and broadly applicable approaches for synthesizing a wide array of bioactive NPs.

Polyphenols are ubiquitous, naturally occurring building blocks that display high binding affinity (through diverse covalent and/or noncovalent interactions) to various materials, including biomacromolecules.[11–13] Therefore, polyphenol-mediated supramolecular complexation holds promise for the efficient preparation and stabilization of bioactive NPs. In the present study, we construct a series of bioactive metal–phenolic NPs (b-MPN NPs) via the one-pot assembly of biomacromolecules, metal ions, and polyphenols (**Figure 1**a).

Poly(ethylene glycol) (PEG) is selected as the seeding agent for the assembly to locally increase the concentration of the metal ion, phenolic ligand, and biomacromolecule precursors. This approach enables the rapid and versatile assembly of a range of bioactive macromolecules, including small-interfering RNA (siRNA) and single or multiple proteins with distinct isoelectric points (ranging from 4.2–10.3) and molecular weights (*M*w, 12.4–240 kDa) (i.e., bovine serum albumin (BSA), cytochrome C (CYC), ribonuclease A (RNase A), glucose oxidase (GOx), and catalase (Cat)), into uniform, spherical structures under mild conditions. Furthermore, the diverse choice of phenolic ligands (i.e., tannic acid (TA), epigallocatechin gallate (EGCG), catechin (CAT), and gallic acid (GA)) and metal ions (i.e., Cu^{II}, Fe^{III}, Al^{III}, Zr^{IV}, and Ti^{IV}) that can be employed highlights the versatility and tunability of the developed b-MPN NP assembly platform. The polyphenols are integral to the assembly process as they exhibit diverse interactions with biomolecules[14] and they stabilize the b-MPN NPs predominantly through hydrophobic and coordination interactions. Notably, all incorporated bioactive macromolecules retain their intrinsic activity, as demonstrated by cancer cell apoptosis, RNA degradation, the decomposition of hydrogen peroxide into oxygen and water, and gene downregulation studies. Finally, the highly adherent nature of the phenolic moieties allows b-MPN NPs to serve as nanoscale building blocks for forming microscale superstructures. The assembly strategy reported here is expected to advance the use of b-MPN NPs for various applications in biotechnology.

2. Results and Discussion

The globular protein commonly found in blood plasma, namely BSA, was first used as a model bioactive macromolecule to assemble b-MPN NPs. Fe^{III} and TA were selected as metal ion and phenolic building blocks, respectively, while PEG served as the seeding agent. Dynamic light scattering (DLS) along with the observation of Tyndall effects (i.e., scattering of a light beam by a media containing suspended colloidal particles) indicated that the

formation of the b-MPN NPs was initiated by the addition of TA to a premixed mixture of PEG, BSA, and Fe^{III} (Figure 1b; inset image 4),[15] which could be attributed to the diverse interactions of the catechol/gallol moieties of TA.[12] Furthermore, the addition of TA and Fe^{III} successively decreased the fluorescence intensity of fluorescein isothiocyanate-tagged BSA due to quenching by TA and chelated Fe^{III} (Figure S1), further indicating the interactions among BSA, TA, and Fe^{III}.[16] The b-MPN NPs (i.e., BSA-MPN NPs) were spherical (~125 nm in diameter) with a relatively narrow size distribution (polydispersity index (PDI) < 0.1; Figure 1b, c; Table S1). Energy dispersive X-ray spectroscopy (EDX) mapping revealed that the NPs were composed of C, O, N, and Fe. Moreover, the appearance of the characteristic ligand-to-metal charge transfer (LMCT) band at ~570 nm suggested the existence of metal–phenolic coordination (Figure 1d).[17]

The size of the NPs was controlled through the choice of *M*w of PEG and metal ion-to-ligand molar ratio. As shown in Figure 1e, the use of longer PEG chains (i.e., higher *M*w) resulted in smaller and less negatively charged NPs, owing to the enhanced degree of cross-linking and shielding.[18] The NP diameter decreased from ~180 to ~45 nm, whereas the ζ-potential increased from –40 to –20 mV upon increasing the *M*w of PEG from 1 to 35 kDa (Figure 1e, S2, Table S2). The size of the NPs initially decreased from ~220 to ~105 nm when the Fe^{III}:TA molar ratio increased from 0 to 1 (Figure S3, Table S3), suggesting that the incorporation of Fe^{III} enhanced the cross-linking density of the NPs. Further addition of Fe^{III} resulted in a gradual increase in the size of NPs and the formation of irregular aggregates, as deduced by the larger PDI determined from the DLS measurements and transmission electron microscopy (TEM) images (Figure S3, S4 and Table S3). NP size tunability may allow b-MPN NPs to encapsulate different sizes of proteins (e.g., larger NPs may allow the encapsulation of larger sizes of proteins) and enable the control of cellular uptake efficiency (e.g., smaller NPs may have more efficient uptake profiles) and intracellular fate of b-MPN NPs.[19] It is noted that increasing the amount of each precursor (i.e., PEG, BSA, Fe^{III}, and

TA) 30-fold while keeping a constant ratio between the components resulted in a higher number of NPs (Figure S5a) without a noticeable change in average size or shape (Figure S5b, S6, Table S4), suggesting that this approach is highly scalable.

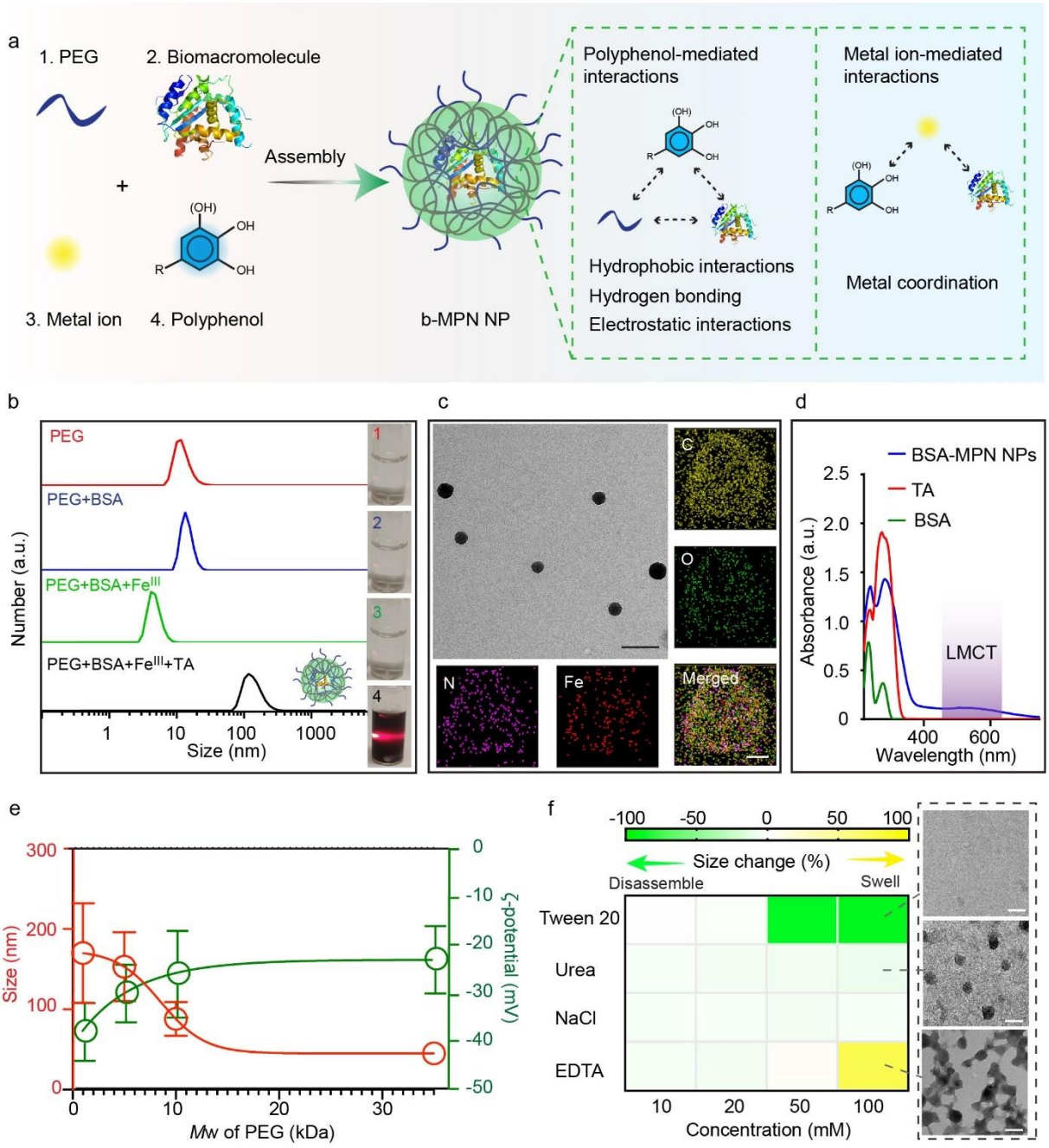

Figure 1. Assembly and disassembly of b-MPN NPs. (a) Schematic illustration of the synthesis of b-MPN NPs via metal–phenolic-mediated assembly. The sequence in which the reagents are added is also indicated. (b) DLS data after adding each component of BSA-MPN NPs. The size reduction of PEG+BSA+Fe^{III} compared to PEG and PEG+BSA is likely due to the enhanced cross-linking density caused by Fe^{III}. Insets are corresponding photographs showing the absence or presence of Tyndall effects. (c) TEM image (scale bar is 200 nm) and EDX mapping (scale bar is 50 nm in all images) of BSA-MPN NPs. (d) UV–vis spectra of free BSA, TA, and BSA-MPN NPs. The purple region highlights the LMCT band in the spectrum of BSA-MPN NPs. (e) Changes in the size and ζ-potential of BSA-MPN NPs in

response to using different *M*w of PEG. (f) Heat map showing the percentage of size change of BSA-MPN NPs after incubation with different solutions. The corresponding TEM images are representative images of BSA-MPN NPs after incubation for 24 h in 100 mM of Tween 20, urea, and EDTA, respectively. Scale bars are 200 nm.

To investigate the dominant interactions governing the stability of the BSA-MPN NPs, urea, Tween 20, NaCl, and ethylenediaminetetraacetic acid (EDTA) were used as dispersants while monitoring the NP size during disassembly. The NPs effectively disassembled after incubation with Tween 20 (≥50 mM), which was likely due to hydrophobic competition.[13] In contrast, the BSA-MPN NPs remained relatively stable after incubation in urea, which is known to disrupt weak hydrogen bonds by participating in the formation of strong hydrogen bonds,[14] or NaCl, which can disrupt ionic interactions,[14] suggesting hydrogen bonding and electrostatic interactions are not the dominant stabilizing forces (Figure 1f). The BSA-MPN NPs swelled to ~180 nm after incubation with 100 mM EDTA (chelating agent;[11b] pH 7) (Figure 1f, Figure S7), which is attributed to the reduced cross-linking density of the NPs after removal of the metal ions[20] and accompanying increase in electrostatic repulsion at pH 7.[21] The relatively small PDI value (<0.2; Table S5), under these conditions, indicated that the increase in NP size was not due to NP aggregation but rather due to swelling.

We next explored the dominant interactions for the stability of the NPs from the perspective of assembly. Therefore, a series of phenolic-based NP systems were prepared as different controls. For example, phenolic NPs obtained by self-assembling TA and PEG were used as biomolecule- and metal ion-free controls. Bioactive phenolic NPs assembled from BSA, TA, and PEG were used as metal ion-free controls. Metal–phenolic NPs synthesized by directly assembling TA, PEG, and Fe^{III} were treated as biomolecule-free controls. Tyndall effects were observed for all of the abovementioned systems (Figure S8), indicating the successful formation of different colloidal NPs. Among the three NP systems, the phenolic NPs showed the largest size and highest polydispersity (i.e., size ≈400 nm, PDI = 0.366; **Figure 2**a, b and Table S6) and the lowest stability (i.e., they rapidly disassembled upon centrifugation). The

bioactive phenolic and metal–phenolic NPs had lower PDIs and average diameters of ~190 and ~130 nm, respectively (Figure 2a, c, d and Table S6), which was likely due to the enhanced cross-linking density of TA with the biomolecules and metal ions. The assembly assay further highlights the key role of polyphenols in NP formation. It is noted that all of the abovementioned NPs effectively disassembled in Tween 20 regardless of the the presence of BSA (Figure S9); however, incubation in EDTA led to complete disassembly of the metal–phenolic NPs. Combining the assembly and disassembly results, multiple interactions (e.g., hydrophobic interactions, coordination, hydrogen bonding, electrostatic interactions) may exist, but the possible dominant modes of interaction within the BSA-MPN NPs are attributed to hydrophobic interactions, with coordination bonding contributing to maintaining the NP size.

To demonstrate the tunability and versatility of b-MPN NPs, we then assembled a series of BSA-MPN NPs with metal ions having different valency and coordination state (i.e., Cu^{II}, Al^{III}, Ti^{IV}, and Zr^{IV}) and phenolic ligands with different sizes (i.e., EGCG, CAT, and GA) (Figure 2e). Using TA as a model polyphenol, all selected metal ions formed b-MPN NPs of ~120 nm in size and featuring ζ-potentials ranging from –30 to –50 mV (Figure 2f, S10a and Table S1). Using Fe^{III} as a model metal ion, the use of smaller phenolic ligands led to the formation of b-MPN NPs with comparable sizes but generally with more neutral ζ-potentials, possibly due to a higher concentration of PEG on the surface (Figure 2g, S10b and Table S7). All synthesized BSA-MPN NPs remained stable in physiologically-relevant buffer solutions (e.g., pH 7 3-(*N*-morpholino)propanesulfonic acid (MOPS) and Dulbecco's phosphate-buffered saline) and the biological conditions studied (e.g., complete Dulbecco's modified Eagle's medium (DMEM) with 10% fetal bovine serum (FBS)) for 4 weeks (Figure S11, S12). Overall, the b-MPN NPs were more stable in slightly alkaline conditions (e.g., from pH 7 to 9) and remained stable in slightly acidic conditions (e.g., pH 5.6 and cell-cultured media; Figure S11b) but had a tendency to aggregate at pH 4. Specifically, at higher pH, the hydroxyl

moieties of polyphenols deprotonate,[21] which enhances electrostatic repulsion while mitigating hydrogen bonding, leading to improved dispersibility. In contrast, in more acidic environments (e.g., pH 4), the polyphenols become more protonated, which may increase the likelihood of hydrogen bonding formation and potentially inducing aggregation. In addition, negligible size changes were observed after exposing b-MPN NPs to different temperatures (i.e., –20 °C, 4 °C, 25 °C, and 37 °C) for 24 h (Figure S13, S14), indicating that the NPs are stable over a wide temperature range.

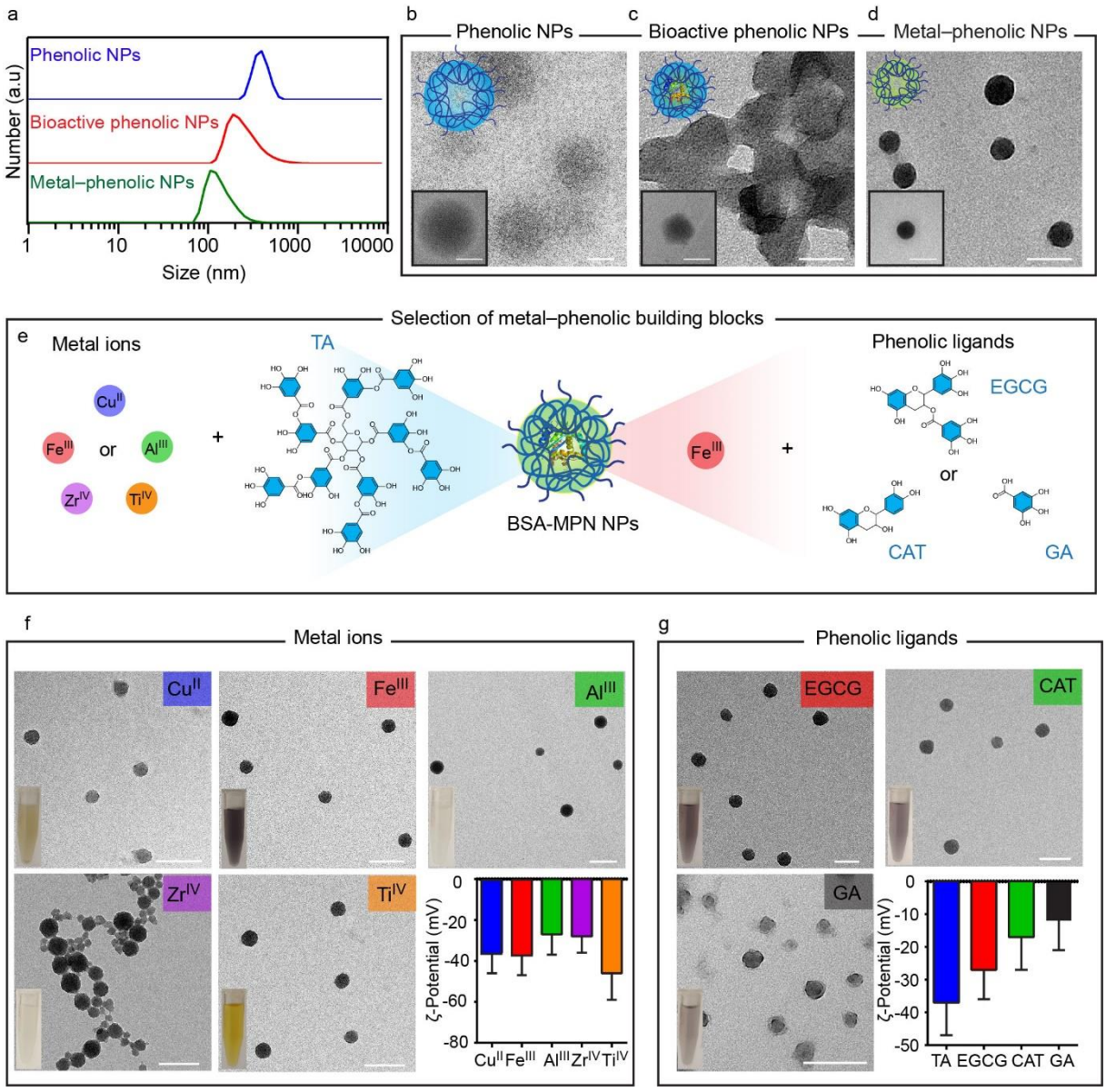

Figure 2. Tunability and versatility of b-MPN NPs using different building blocks. (a–d) Characterization data of different control NP systems, i.e., phenolic NPs (without metal or bioactive molecules), bioactive phenolic NPs (without metal), and metal–phenolic NPs (without bioactive molecules): DLS (a) and TEM (b–d). (e) Schematic illustration of the

synthesis of BSA-MPN NPs using different metal ions and phenolic building blocks. TEM images (scale bars are 200 nm) and ζ-potential of (f) BSA-MPN NPs assembled from TA and different metal ions and (g) BSA-MPN NPs assembled from Fe^{III} and different phenolic ligands.

Several other biomacromolecules, such as proteins and genes, were successfully incorporated into the b-MPN NPs without impairing their biological activity. CYC and RNase A were selected for their respective cell apoptosis and RNA degradation activities and assembled into CYC-MPN NPs and RNase A-MPN NPs using EGCG and Zr^{IV} (**Figure 3**a). The CYC-MPN NPs and RNase MPN NPs displayed diameters of ~120 and ~140 nm, respectively, a relatively uniform size distribution, and a net negative charge in pH 7.4 MOPS buffer solution and complete media (DMEM with 10% FBS) (Figure S15–S17 and Table S8). The apoptotic activity of CYC was monitored by evaluating the viability of MDA-MB-231 breast cancer cells at different concentrations. As observed from Figure 3b, CYC-MPN NPs induced ~80% cell death at an effective protein concentration of 160 μg mL^{-1}, whereas the CYC control (i.e., free CYC) led to negligible cell death due to a lack of cellular uptake and/or intracellular trafficking.[22] The release of proteins might be triggered by the disassembly of metal–phenolic complexes and the intracellular glutathione/glutathione disulfide (through competing supramolecular interactions).[22] BSA-MPN NPs, which contain proteins without apoptotic function, also demonstrated negligible cytotoxicity (Figure S18), highlighting that the functionality of the NPs can be easily tuned through the choice of the biomolecule. Notably, the metal ion-free controls (i.e., NPs assembled from CYC, EGCG, and PEG in the absence of Zr^{IV}) also induced cell death but with significantly lower efficiency in comparison with CYC-MPN NPs (Figure 3b), likely because the absence of metal ions and metal–phenolic coordination reduced the endosomal escape capability of the NPs.[23] The preservation of RNase A activity was also confirmed (Figure 3c), where RNase A-MPN NPs displayed the highest efficacy (i.e., ~85% cell death) among the metal ion-free controls (i.e., ~4-fold lower) and RNase A controls (~5-fold lower) (Figure 3d).

Moreover, multifunctional b-MPN NPs were engineered by incorporating multiple bioactive macromolecules into a single NP platform. For example, Cat was co-assembled with GOx to form (GOx-Cat)-MPN NPs to eliminate toxic intermediates via cascade reactions (Figure 3e). Oxidase has been proposed for various cancer therapies relying on starvation of cancer cells;[24] however, H_2O_2 that is generated from oxidase-mediated reactions is harmful to healthy cells.[25] Incorporating Cat with GOx can generate a biocatalytic cascade event that can promote the breakdown of H_2O_2 to O_2, thereby attenuating tumor hypoxia and further improving O_2-dependent therapy modalities.[26] Incubating cells with GOx-MPN NPs in a glucose-containing media caused ~90% cell death after 48 h. Subsequent addition of the same amount of Cat-MPN NPs into the media after 6 h improved cell viability to 65%. In contrast, treating cells with (GOx-Cat)-MPN NPs further improved cell viability to >95% (Figure 3f). These multifunctional NPs not only exhibit the robustness and versatility (in relation to the incorporation of diverse cargos) of b-MPN NPs, but also offer a route to engineer complex biomimetic systems.

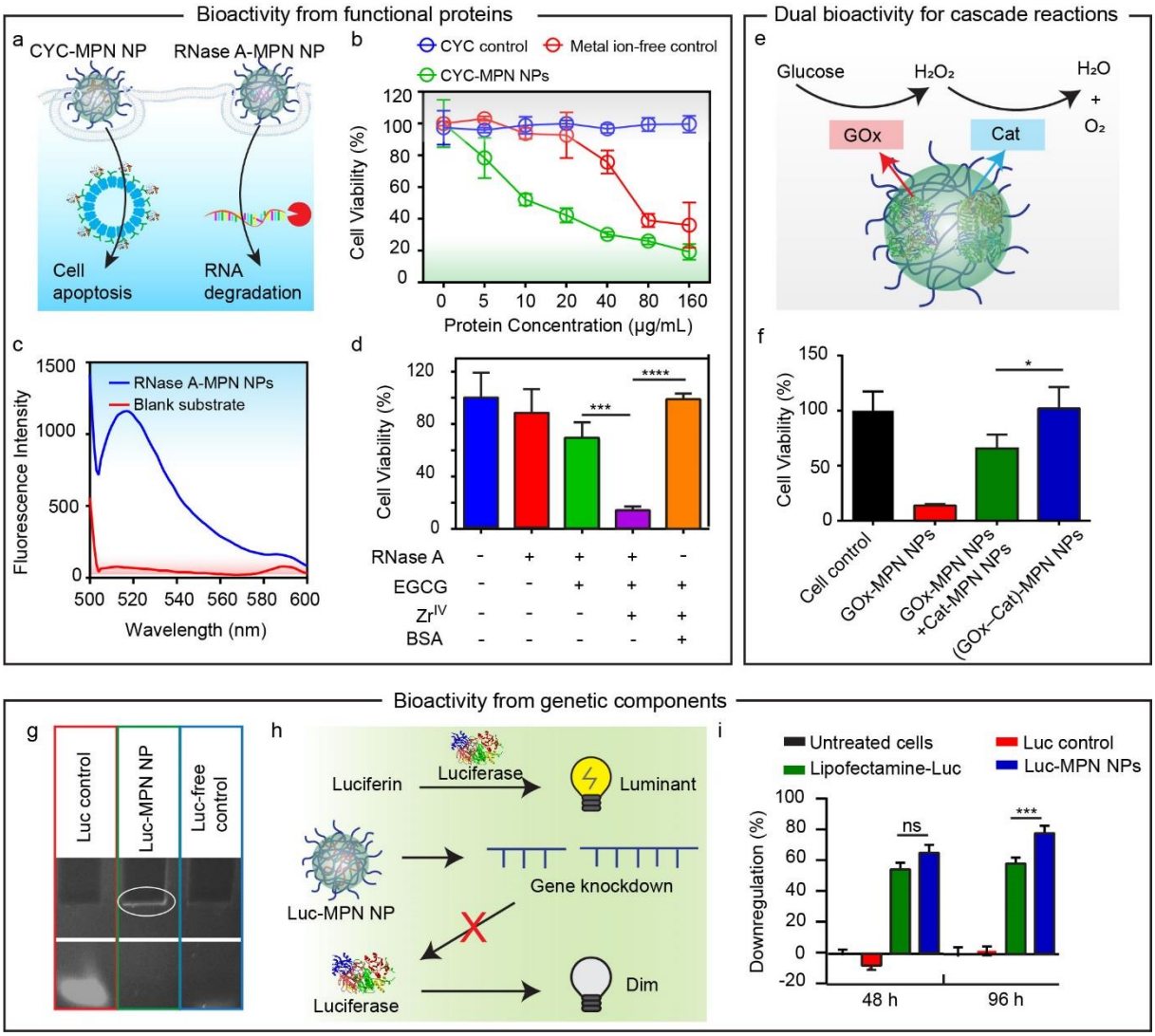

Figure 3. Bioactivity of b-MPN NPs composed of different biomacromolecules. (a) Schematic illustration of applying bioactive CYC-MPN NPs and RNase A-MPN NPs for cell apoptosis and RNA degradation. (b) Protein concentration-dependent cell viability of MDA-MB-231 cells incubated with free CYC control, metal ion-free controls (NPs prepared from PEG, CYC, and EGCG), and CYC-MPN NPs in complete DMEM (with 10% FBS) for 48 h at 37 °C. (c) Enzymatic activity of a blank substrate (fluorescent substrate is a modified RNA oligonucleotide that emits green fluorescence when it is cleaved by RNase) from the RNaseAlert Lab Test Kit and the substrate following incubation with RNase A-MPN NPs. (d) Cell viability of untreated MDA-MB-231 cells and cells incubated with free RNase A, metal ion-free NPs, and RNase A-MPN NPs, and BSA-MPN NPs (prepared from EGCG and Zr^{IV}) in complete DMEM (with 10% FBS) for 48 h at 37 °C. (e) Schematic illustration of the cascade reaction enabled by multifunctional (GOx-Cat)-MPN NPs. (f) Cell viability of untreated MDA-MB-231 cells (Cell control) and cells incubated with GOx-MPN NPs, a mixture of GOx-MPN NPs and Cat-MPN NPs, and (GOx-Cat)-MPN NPs in complete DMEM (with 10% FBS) for 48 h at 37 °C. *$p < 0.1$ with 95% confidence level from unpaired *t*-test. (g) TBE polyacrylamide gel electrophoresis of free Luc siRNA (Luc control), Luc-MPN NPs, and Luc-free NPs (Luc-free control). (h) Schematic illustration of Luc working mechanisms and RNA interference using Luc-MPN NPs. (i) Luc gene knockdown in PC3-Luc cells 48 and 96 h after transfection. ns, not significantly different; ***$p < 0.001$ with 95% confidence level from unpaired *t*-test.

RNA-based therapeutics (e.g., siRNA) have also emerged as promising agents to alter gene functions in various disease treatments.[27] Therefore, integrating the bioactivity of genetic compounds could further expand the use of b-MPN NPs. Luciferase (Luc) siRNA was assembled into NPs (i.e., Luc-MPN NPs), and the bioactivity was evaluated by monitoring the percentage of gene downregulation. The Luc-MPN NPs were ~80 nm in size (Figure S19), and the incorporation of siRNA with other substrates was validated by 10% tris-borate-EDTA (TBE) polyacrylamide gel electrophoresis. Compared to free Luc siRNA that displayed a distinct and bright band in the gel, the mobility of the Luc-MPN NPs was inhibited in the gel loading well, implying successful incorporation of Luc into NPs (Figure 3g). For the gene downregulation study, PC3 cells expressing the firefly luciferase gene (PC3-Luc2) were used. Luc can catalyze luciferin into luminescent products (Figure 3h), allowing monitoring of gene downregulation. As the luminescence intensity was strongly dependent on the amount of Luc inside the cell, gene downregulation was determined through a luminescence assay at different time points. Specifically, 80% of protein expression was silenced by Luc-MPN NPs up to 96 h after transfection (Figure 3i), which is comparable to commercial cationic lipid-mediated transfection agent Lipofectamine RNAiMax (Lipofectamine-Luc in Figure 3i). Collectively, these results suggest that the present assembly strategy retains the bioactivity of the genetic components.

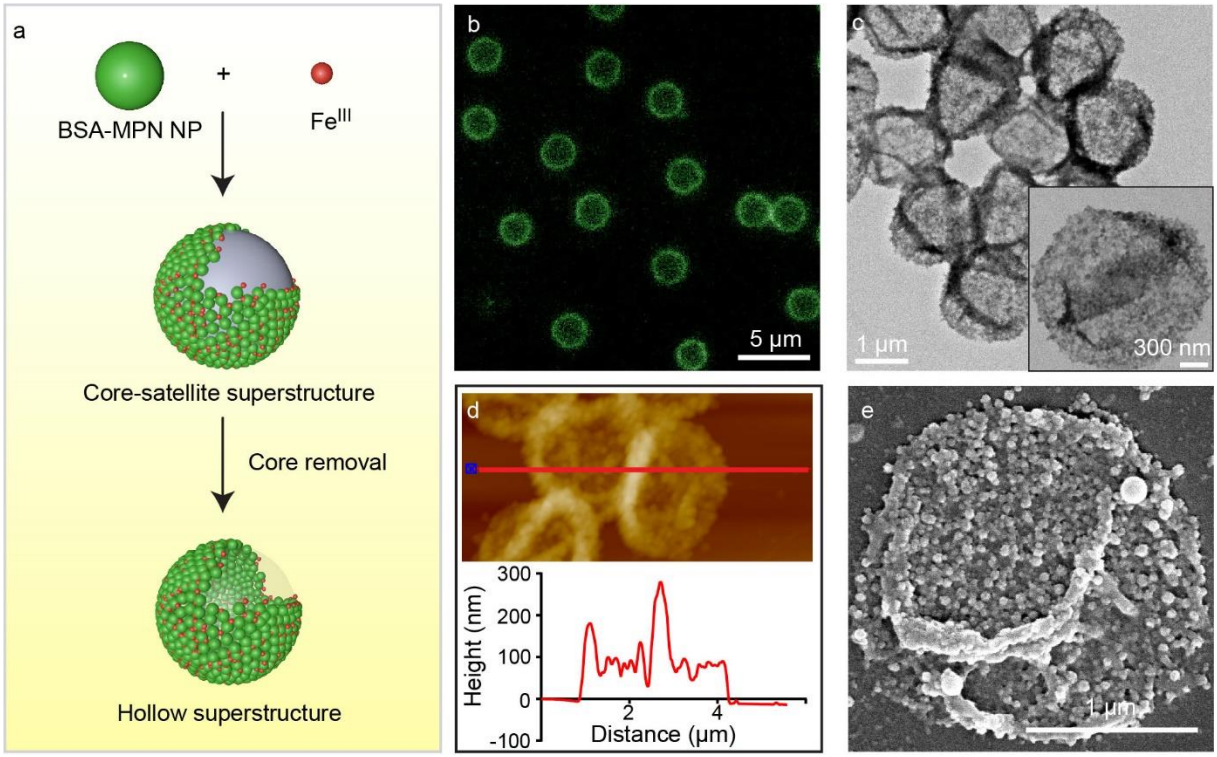

Figure 4. Superstructure assembly of b-MPN NPs. (a) Schematic illustration of the formation of superstructures from BSA-MPN NP building blocks. (b) Fluorescence microscopy images of hollow superstructures after degradation of the sacrificial PS template. (c) TEM images of hollow superstructures. (d) Atomic force microscopy image of hollow superstructures in the air-dried state and the corresponding thickness profile of the superstructures determined across the red line shown in the atomic force microscopy image. (e) Scanning electron microscopy image of a single hollow superstructure demonstrating the surface features of the NP. A suspension of the hollow superstructures was allowed to air dry prior to imaging.

The relatively uniform size and the presence of multidentate polyphenols within the b-MPN NPs suggest that the b-MPN NPs may serve as nanoscale building blocks for the formation of microscale superstructures. For example, superstructures were constructed by mixing BSA-MPN NPs with larger templates (e.g., carboxyl-functionalized polystyrene particles with a size of 1.86 ± 0.03 μm; Figure S20a) followed by the addition of metal ions to instigate metal–phenolic coordination between the b-MPN NPs to anchor them in place (**Figure 4**a), similar to previously reported metal–phenolic superstructures.[28] Intact hollow structures (capsules) were observed under fluorescence microscopy and differential interference contrast microscopy after template core removal (Figure 4b and S20b, respectively), confirming the interconnectivity of the NP building blocks. Collapsed capsules with creased and granular

surface features were visible in the air-dried samples under TEM and atomic force microscopy (Figure 4c, d). Scanning electron microscopy demonstrated that the NP building blocks were densely packed within the capsules (Figure 4e). Collectively, these results demonstrate the versatility of b-MPN NPs as building blocks for further engineering complex architectures. These and related b-MPN NP superstructures and detailed examination of their biological activities and functions are the subject of future studies.

3. Conclusion

We have reported a robust approach to construct b-MPN NPs via supramolecular assembly predominantly driven by hydrophobic interactions and metal–phenolic coordination. The b-MPN NPs exhibited negligible cytotoxicity when incorporated with nontoxic bioactive agents (e.g., BSA) but could readily be constructed from individual or combinations of other bioactive macromolecules to exhibit specific biological functionality. The diverse choice of biomacromolecules, phenolic ligands, and metal ions available for engineering afforded a library of functional NPs, performing in a range of applications such as cell apoptosis, RNA degradation, catalysis, and gene silencing. Additionally, the phenolic motifs on the surface of the b-MPN NPs enabled the use of the b-MPN NP as building blocks to form superstructures. The bioactivity in terms of both function and structure, along with the tunability and versatility, of the NP platform presented, are expected to advance both fundamental and applied research in the development and application of engineered NPs in bionanotechnology and related fields.

Supporting Information

Supporting Information is available from the Wiley Online Library or from the author.

Acknowledgements

This research was conducted and funded by an Australian Research Council Discovery Project (DP200100713). F.C. acknowledges the award of a National Health and Medical

Research Council Senior Principal Research Fellowship (GNT1135806). This work was performed in part at the Materials Characterisation and Fabrication Platform (MCFP), Biosciences Microscopy Unit at The University of Melbourne, and the Victorian Node of the Australian National Fabrication Facility (ANFF). Transmission electron microscopy and energy-dispersive X-ray spectroscopy experiments were conducted at the Bio21 Advanced Microscopy Facility, The University of Melbourne. The authors acknowledge Dr. Sukhvir Kaur Bhangu, Dr. Chan-Jin Kim, Dr. Yingjie Hu, Shiyao Li, and Wanjun Xu for helpful discussions.

Conflict of Interest

The authors declare no competing financial interests.

Received: ((will be filled in by the editorial staff))
Revised: ((will be filled in by the editorial staff))
Published online: ((will be filled in by the editorial staff))

References

[1] a) T. Hueckel, G. M. Hocky, S. Sacanna, *Nat. Rev. Mater.* **2021**, https://doi.org/10.1038/s41578-021-00323-x; b) L. R. MacFarlane, H. Shaikh, J. D. Garcia-Hernandez, M. Vespa, T. Fukui, I. Manners, *Nat. Rev. Mater.* **2020**, *6*, 7; c) W. B. Rogers, W. M. Shih, V. N. Manoharan, *Nat. Rev. Mater.* **2016**, *1*, 1; d) N. Vogel, M. Retsch, C. A. Fustin, A. d. Campo, U. Jonas, *Chem. Rev.* **2015**, *115*, 6265.

[2] a) M.-S. Balogun, W. Qiu, Y. Luo, Y. Huang, H. Yang, M. Li, M. Yu, C. Liang, P. Fang, P. Liu, Y. Tong, *ChemElectroChem* **2015**, *2*, 1243; b) L. Dai, *Acc. Chem. Res.* **2013**, *46*, 31.

[3] a) M. Ha, J.-H. Kim, M. You, Q. Li, C. Fan, J.-M. Nam, *Chem. Rev.* **2019**, *119*, 12208; b) L. Gloag, M. Mehdipour, D. Chen, R. D. Tilley, J. J. Gooding, *Adv. Mater.* **2019**, *31*, 1904385.

[4] a) Y. Yin, Z. Tan, L. Hu, S. Yu, J. Liu, G. Jiang, *Chem. Rev.* **2017**, *117*, 4462; b) O. P. Bolade, A. B. Williams, N. U. Benson, *Environ. Nanotechnol. Monit. Manage.* **2020**, *13*, 100279.

[5] a) J. Cui, J. J. Richardson, M. Bjornmalm, M. Faria, F. Caruso, *Acc. Chem. Res.* **2016**, *49*, 1139; b) W. He, X. Xing, X. Wang, D. Wu, W. Wu, J. Guo, S. Mitragotri, *Adv. Funct. Mater.* **2020**, *30*, 1910566; c) J. N. Liu, W. B. Bu, J. L. Shi, *Acc. Chem. Res.* **2015**, *48*, 1797.

[6] a) J. Chang, X. Chen, Z. Glass, F. Gao, L. Mao, M. Wang, Q. Xu, *Acc. Chem. Res.* **2019**, *52*, 665; b) J. Wang, Y. Li, G. Nie, *Nat. Rev. Mater.* **2021**, *6*, 766.

[7] a) D. Ling, T. Hyeon, *Small* **2013**, *9*, 1450; b) Z. He, P. Alexandridis, *Phys. Chem. Chem. Phys.* **2015**, *17*, 18238.

[8] a) Y.-W. Lee, D. C. Luther, R. Goswami, T. Jeon, V. Clark, J. Elia, S. Gopalakrishnan, V. M. Rotello, *J. Am. Chem. Soc.* **2020**, *142*, 4349; b) K. Dutta, D. Hu, B. Zhao, A. E. Ribbe, J. Zhuang, S. Thayumanavan, *J. Am. Chem. Soc.* **2017**, *139*, 5676; c) J. Lv, Q. Fan, H. Wang, Y. Cheng, *Biomaterials* **2019**, *218*, 119358.

[9] a) K. L. Gurunatha, A. C. Fournier, A. Urvoas, M. Valerio-Lepiniec, V. Marchi, P. Minard, E. Dujardin, *ACS Nano* **2016**, *10*, 3176; b) J. Zhang, K. Zhou, Y. Zhang, M. Du, Q. Wang, *Adv. Mater.* **2019**, *31*, 1901485.

[10] a) L. Ren, J. Lv, H. Wang, Y. Cheng, *Angew. Chem. Int. Ed.* **2020**, *59*, 4711; b) C. J. Wilson, A. S. Bommarius, J. A. Champion, Y. O. Chernoff, D. G. Lynn, A. K. Paravastu, C. Liang, M.-C. Hsieh, J. M. Heemstra, *Chem. Rev.* **2018**, *118*, 11519; c) Q. Luo, C. Hou, Y. Bai, R. Wang, J. Liu, *Chem. Rev.* **2016**, *116*, 13571.

[11] a) D. Wu, J. Zhou, M. N. Creyer, W. Yim, Z. Chen, P. B. Messersmith, J. V. Jokerst, *Chem. Soc. Rev.* **2021**, *50*, 4432; b) H. Ejima, J. J. Richardson, K. Liang, J. P. Best, M. P. van Koeverden, G. K. Such, J. Cui, F. Caruso, *Science* **2013**, *341*, 154; c) W. Shen, Q. Wang, Y. Shen, X. Gao, L. Li, Y. Yan, H. Wang, Y. Cheng, *ACS Cent. Sci.* **2018**, *4*, 1326.

[12] J. Zhou, Z. Lin, Y. Ju, M. A. Rahim, J. J. Richardson, F. Caruso, *Acc. Chem. Res.* **2020**, *53*, 1269.

[13] J. E. Chung, S. Tan, S. J. Gao, N. Yongvongsoontorn, S. H. Kim, J. H. Lee, H. S. Choi, H. Yano, L. Zhuo, M. Kurisawa, J. Y. Ying, *Nat. Nanotechnol.* **2014**, *9*, 907.

[14] Y. Han, Z. Lin, J. Zhou, G. Yun, R. Guo, J. J. Richardson, F. Caruso, *Angew.Chem. Int. Ed.* **2020**, *59*, 15618.

[15] H. Yao, W. Liu, L. Lin, Y. Lu, J.-H. Gan, Y. Liu, N.-P. Tao, X.-C. Wang, M.-S. Hong, C.-H. Xu, *Food Chem.* **2021**, *342*, 128383.

[16] C. Liu, W. Shen, B. Li, T. Li, H. Chang, Y. Cheng, *Chem. Mater.* **2019**, *31*, 1956.

[17] S. Pan, R. Guo, N. Bertleff-Zieschang, S. Li, Q. A. Besford, Q. Z. Zhong, G. Yun, Y. Zhang, F. Cavalieri, Y. Ju, E. Goudeli, J. J. Richardson, F. Caruso, *Angew.Chem. Int. Ed.* **2020**, *59*, 275.

[18] a) C. L. Jenkins, H. J. Meredith, J. J. Wilker, *ACS Appl. Mater. Interfaces* **2013**, *5*, 5091; b) M. Amirilargani, A. Sabetghadam, T. Mohammadi, *Polym. Adv. Technol.* **2012**, *23*, 398.

[19] a) J. Mosquera, I. Garcia, L. M. Liz-Marzan, *Acc. Chem. Res.* **2018**, *51*, 2035; b) S. Behzadi, V. Serpooshan, W. Tao, M. A. Hamaly, M. Y. Alkawareek, E. C. Dreaden, D. Brown, A. M. Alkilany, O. C. Farokhzad, M. Mahmoudi, *Chem. Soc. Rev.* **2017**, *46*, 4218.

[20] H. Li, P. Yang, P. Pageni, C. Tang, *Macromol. Rapid Commun.* **2017**, *38*, 1700109.

[21] J. Chen, S. Pan, J. Zhou, Q. Z. Zhong, Y. Qu, J. J. Richardson, F. Caruso, *Chem. Mater.* **2020**, *32*, 6975.

[22] Y. Han, J. Zhou, Y. Hu, Z. Lin, Y. Ma, J. J. Richardson, F. Caruso, *ACS Nano* **2020**, *14*, 12972.

[23] J. Chen, J. Li, J. Zhou, Z. Lin, F. Cavalieri, E. Czuba-Wojnilowicz, Y. Hu, A. Glab, Y. Ju, J. J. Richardson, F. Caruso, *ACS Nano* **2019**, *13*, 11653.

[24] C. Wang, J. Yang, C. Dong, S. Shi, *Adv. Ther.* **2020**, *3*, 2000110.

[25] Y. Liu, J. Du, M. Yan, M. Y. Lau, J. Hu, H. Han, O. O. Yang, S. Liang, W. Wei, H. Wang, J. Li, X. Zhu, L. Shi, W. Chen, C. Ji, Y. Lu, *Nat. Nanotechnol.* **2013**, *8*, 187.

[26] M. Wang, D. Wang, Q. Chen, C. Li, Z. Li, J. Lin, *Small* **2019**, *15*, 1903895.

[27] a) J. Gilleron, W. Querbes, A. Zeigerer, A. Borodovsky, G. Marsico, U. Schubert, K. Manygoats, S. Seifert, C. Andree, M. Stoter, H. Epstein-Barash, L. Zhang, V. Koteliansky, K. Fitzgerald, E. Fava, M. Bickle, Y. Kalaidzidis, A. Akinc, M. Maier, M. Zerial, *Nat. Biotechnol.* **2013**, *31*, 638; b) W. Tai, J. Li, E. Corey, X. Gao, *Nat. Biomed. Eng.* **2018**, *2*, 326.

[28] J. Guo, B. L. Tardy, A. J. Christofferson, Y. Dai, J. J. Richardson, W. Zhu, M. Hu, Y. Ju, J. Cui, R. R. Dagastine, I. Yarovsky, F. Caruso, *Nat. Nanotechnol.* **2016**, *11*, 1105.

A versatile and tunable strategy is developed to assemble a range of biomacromolecules into bioactive metal–phenolic nanoparticles (b-MPN NPs), while retaining the intrinsic activity of the biomacromolecules. The bioactivity of the b-MPN NPs enables their use in various applications, including cell apoptosis, RNA degradation, cascade reactions, and gene silencing.

J. Chen, S. Pan, J. Zhou, Z. Lin, Y. Qu, A. Glab, Y. Han, J. J. Richardson, F. Caruso*

Assembly of Bioactive Nanoparticles via Metal–Phenolic Complexation